Journal of Materials Chemistry

Cite this: J. Mater. Chem., 2012, 22, 7323

www.rsc.org/materials

PAPER

Labeling and monitoring the distribution of anchoring sites on functionalized CNTs by atomic layer deposition†

Catherine Marichy,[a] Jean-Philippe Tessonnier,[b] Marta C. Ferro,[c] Kyeong-Hwan Lee,[d] Robert Schlögl,[e] Nicola Pinna*[ad] and Marc-Georg Willinger*[ae]

Received 27th October 2011, Accepted 2nd February 2012
DOI: 10.1039/c2jm00088a

The chemical inertness of graphite and, in the case of tubes, of rolled up few layer graphene sheets, requires some degree of "defect engineering" for the fabrication of carbon based heterostructured materials. It is shown that atomic layer deposition provides a means to specifically label anchoring sites and can be used to characterize the surface functionality of differently treated carbon nanotubes. Direct observation of deposited titania by analytical transmission electron microscopy reveals the location and density of anchoring sites as well as structure related concentrations of functional groups on the surface of the tubes. Controlled functionalization of the tubes therefore allows us to tailor the distribution of deposited material and, hence, fabricate complex heterostructures.

Introduction

Atomic layer deposition (ALD) provides an elegant, efficient and well controllable way to coat high aspect ratio nanostructures with a homogeneous and conformal film of precisely defined thickness.[1–3] As such, it is ideally suited for the fabrication of complex heterostructures and functional materials.[4–6] Due to their outstanding properties, carbon nanotubes (CNTs) constitute ideal components for such heterostructures. As a matter of fact, ALD has already been successfully applied for the coating of CNTs.[7–16] However, since the initiation of film growth requires the presence of functional surface groups and defect sites that act as anchoring and nucleation sites,[17,18] the inert nature of high quality tubes with a graphitic surface leads to non- or incomplete coating. Depending on the density and nature of functional surface species principally two ALD growth modes can be expected.[3] If the density of surface anchoring sites is high enough to allow the ALD precursors to react completely with the substrate, a 2D growth mode is favored. Otherwise, an island growth mode is favored. In this case, deposition occurs preferentially onto the ALD material already deposited in preceding cycles. In intermediate cases, the growth mode may be first island growth, and when the islands have coalesced to form a continuous layer, 2D growth may occur. Therefore, controlled tailoring of the type, degree and density of functionalization of the CNT surface would allow tuning the coating from selective decoration up to fully coated. This is certainly of interest for applications requiring functional materials based on heterostructured CNTs. Principally, two types of surface functionalization can be distinguished: covalent and non-covalent. The most commonly employed prior to ALD is the covalent functionalization by treatment of pristine CNTs with mineral acids such as HNO_3 or other strong oxidizing agents (*e.g.* O_3). It permits generation of oxygenated functional surface groups such as alcohol, ketone, ether, carboxylic acid and ester, which paves the way to an endless possibility of further attachment.[19,20] On the other hand, non-covalent functionalization is mainly based on supramolecular complexation using various adsorptive and anchoring forces, such as van der Waals and π–π interactions, hydrogen bonding and electrostatic forces. As a prominent example, defect free suspended SWCNTs could be conformally coated with Al_2O_3 by ALD, after a NO_2 pretreatment. In this case, NO_2, which reversibly physisorbs on the SWNTs, acts as an anchoring site for further oxide growth.[12,13]

The study of the location of defects on CNTs was already carried out using different approaches either for labeling or for monitoring. Labeling can be pursued by several techniques such as electrodeposition,[21] nanoparticle attachment in solution[22,23] and exposure to gas phase reactants.[24] Each of these techniques shows some limitations in terms of accuracy; nanoparticles can be also deposited onto an unfunctionalized part of the nanotube and not all of the functional groups would react with a nanoparticle, or in the case of processing, electrodeposition requires

[a]*Department of Chemistry, CICECO, University of Aveiro, 3810-193 Aveiro, Portugal. E-mail: pinna@ua.pt*
[b]*Department of Chemical Engineering, University of Delaware, Newark, DE 19716, USA*
[c]*Department of Ceramics and Glass Engineering, CICECO, University of Aveiro, 3810-193 Aveiro, Portugal*
[d]*World Class University (WCU) program of Chemical Convergence for Energy & Environment (C2E2), School of Chemical and Biological Engineering, College of Engineering, Seoul National University (SNU), Seoul 151-744, Korea. E-mail: pinna@snu.ac.kr*
[e]*Department of Inorganic Chemistry, Fritz Haber Institute of the Max Planck Society, Berlin, Germany. E-mail: willinger@fhi-berlin.mpg.de*
† Electronic supplementary information (ESI) available. See DOI: 10.1039/c2jm00088a

the CNTs to be contacted at multiple positions by lithography, for example. Furthermore, monitoring defects by spectroscopy techniques *e.g.* Raman[25] or photoluminescence[23] does not offer a spatial resolution high enough to map the defects at the nanometre scale. Alternative techniques that provide atomic resolution such as STM or AFM are limited in the study of complex nanostructured materials and allow only scanning a small region of the sample.[21,22]

In this manuscript we will demonstrate that ALD, in combination with high resolution and analytical transmission and scanning electron microscopies, appears as the technique of choice to map anchoring sites on nanostructured supports and to study the distribution of functional groups as a function of structure and functionalization treatment.

Experimental section

Carbon nanotube chemical treatments and chemical characterizations

Stacked-cups carbon nanotubes were purchased from Pyrograf Products (USA). The CNTs were synthesized by catalytic chemical vapor deposition (CCVD) using the floating catalyst method described in detail elsewhere.[26] Briefly, CH_4 and $Fe(CO)_5$ were fed simultaneously in a horizontal reactor maintained at 1100 °C. The thermal decomposition of the iron precursor generated iron nanoparticles which subsequently catalyzed the growth of the nanotubes. Because of the high reaction temperature, methane was also decomposed thermally (pyrolysis) on the CNT walls, leaving a relatively thick layer of disordered pyrolytic carbon.

After synthesis, the CNTs were heat treated in inert atmosphere at either 700 °C (product PR24-PS), 1500 °C (PR24-LHT) or 3000 °C (PR24-HHT) in order to graphitize the layer of pyrolytic carbon, hence decreasing the density of structural defects in a controlled manner. The CNTs exhibit average outer and inner diameters of 85 and 40 nm, respectively, independently of the applied annealing temperature. The three commercial products were subsequently oxidized with concentrated nitric acid (70%) at 100 °C for 10 h. The temperature was deliberately kept low, significantly under the boiling point of HNO_3 (120 °C) in order to prevent any structural damage to the CNTs which could modify their structural properties. The mixture was then allowed to cool down to room temperature and the functionalized CNTs were filtered and rinsed with 1 L distilled water. For the sake of clarity, the oxidized PR24-PS, PR24-LHT and PR24-HHT samples were labeled CNT700, CNT1500 and CNT3000. Part of the CNT700 sample was further heat treated in Ar at 800 °C to remove a fraction of the oxygen-containing functional groups. This sample was labeled CNT700D (defunctionalized). With increasing annealing temperature, the degree of graphitization of the surface rises and as a consequence, the impact of the classic nitric acid treatment on the functionalization of the wall surface is altered. The TG-MS and XPS characterizations revealed that the formation of carboxylic acid and anhydrides, which typically are the most abundant functional groups for this kind of oxidizing treatment, seems to be disfavored when the structural order of the carbon material increases (Table 1).[27] As a consequence, the pH of aqueous dispersions of CNT700 and CNT1500 increases, and the CNT3000 solution eventually turns basic. In addition, the concentration of surface functional groups created during the HNO_3 treatment decreases when increasing the graphitization temperature, as a result of the lower defect density (as observed from the evolution of the D/G ratio in Raman spectra, *cf.* ref. 27 and Table 1). An alternative modification of the nature and density of surface groups was achieved through a partial defunctionalization of the CNT700 sample in Ar at 800 °C. This post-treatment removes 89% of the oxygen, as determined by XPS, but without significant increase of the defect density.[27]

Table 1 Characterization of the CNTs used in this work: carboxylic acid and phenol concentration determined by acid–base titration with NaOH (in μmol g^{-1}), total oxygen concentration determined by XPS and D/G ratios calculated from Raman spectra. Data taken from ref. 24

Sample name	Carboxylic acid[a]	Phenols[a]	O/C[b]	I_D/I_G[c]
CNT700	130	180	0.099	3.6
CNT1500	27	32	0.12	1.0
CNT3000	0	18	0.05	~0
CNT700D	0	22	0.011	

[a] Determined by acid–base titration. [b] Measured by XPS. [c] Calculated from Raman spectra on CNT materials prior to acid treatment.

Atomic layer deposition and structural characterizations

Titanium dioxide was deposited simultaneously on the CNTs exposed to the various treatments and on a silicon wafer. The latter was used as a reference substrate for film thickness measurement. Prior to the ALD, CNTs were deposited by drop-deposition on a silicon wafer from dispersions in ethanol. In order to remove the ethanol adsorbed at the surface of the CNTs, the samples were treated at 200 °C at 1 mbar under a stream of nitrogen for 15 min inside the ALD chamber prior to the first deposition cycle. The four types of carbon material were inserted and coated at the same time, in the same chamber, in order to have exactly the same deposition conditions. Titanium isopropoxide and acetic acid were used as metal and oxygen sources, respectively. The depositions took place at 200 °C in an ALD reactor operated in exposure mode. Metal precursor and acetic acid were introduced subsequently by pneumatic ALD valves from their reservoirs, which were kept at 80 and 30 °C, respectively. Pure nitrogen was used as a carrier gas at a constant flow rate of 5 sccm. The ALD valves were opened for 0.03 and 1.2 s for the oxygen source and titanium precursor, respectively. The residence time after each precursor pulse was set to 20 s, followed by a nitrogen purge for 15 s. In order to study the nucleation of the oxide and to monitor the growth behavior as a function of the density of functional surface groups, different numbers of ALD cycles were realized in order to deposit various thicknesses. The number of cycles was chosen between 25 and 1000 with a nominal growth per cycle (GPC) of 0.6 Å.[28]

The thickness of the as deposited titanium dioxide films on the wafer substrates was measured by X-ray reflectivity (XRR) using a Philips X'Pert MRD X-ray diffractometer with a copper radiation and a graphite monochromator for the selection of pure Kα radiation. The X-ray tube was operated at 20 kV and

20 mA. A 1 mm slit was used in order to reduce the scattered X-ray intensity. Measurements were performed in a low-resolution experimental set up with the following instrumental configuration: divergence slit at the incident beam: 1/8 in.; step width: 0.01°; and acquisition time: 1 s.

CNTs were characterized before and after ALD of TiO_2 by high-resolution transmission electron microscopy (HRTEM) and scanning transmission electron microscopy (STEM) using a JEOL JEM-2200FS, a Hitachi H9000 and a Philips CM200 FEG microscope. Electron energy loss spectra (EELS) were also recorded from the coated carbon nanotubes. Scanning electron microscopy (SEM) images were recorded using a FEG-SEM Hitachi SU-70 microscope operating at 4 kV with a working distance of 2–3 mm. SEM and TEM investigations were carried out on copper TEM grids with a holey carbon support film. The samples were deposited by dipping the TEM grids into dry powder.

Results and discussion

Commercial stacked-cup CNTs possess several main advantages over other nanocarbons for the present work and were therefore chosen as a starting material. First, the as-grown CNTs are wrapped with a layer of pyrolytic carbon which finds its origin in the particular synthesis conditions of these CNTs. This layer consists of small graphene sheets, so-called basic structural units (BSUs), which are only a few nm in size. They are interconnected by sp^2 and sp^3 carbon chains and assembled in concentric layers. From a structural and chemical point of view, the layer of pyrolytic carbon can be seen as a model surface representative of various nanocarbons such as carbon nanofibers, SWCNTs and MWCNTs, which allows us to extend the scope and the impact of this work. Tessonnier *et al.* used the same stacked-cup CNTs as a model material to develop a technique to selectively deposit metal particles either inside or outside CNTs.[29] This selective deposition technique has been successfully employed by different groups on various CNTs since then.[30–32] Secondly, the layer of pyrolytic carbon exhibits a high concentration of structural defects (see below) which can be tuned by annealing in an inert atmosphere (graphitization). Therefore, these materials offer a large playground to study the effect of the defect density and of the surface chemistry on the ALD. Finally, it was demonstrated that MWCNTs exhibit a large number of carbonaceous debris on their surface, which are hard to characterize, but which significantly interfere during the functionalization,[33] or the use of the MWCNTs in catalytic reactions.[34] In contrast, the surface of the stacked-cup CNTs is well defined.[27]

The high resolution transmission electron micrographs (HRTEMs) nicely show the evolution of the structural defects and of the graphitization as a function of annealing temperature (*cf.* ref. 35). The CNT700 is characterized by a structural disorder of the outer and inner surface layer of the tubes (Fig. 1a and b). The annealing at 1500 °C prior to the nitric acid treatment leads to the appearance of some connections between the inner rims of subsequently stacked cups (see arrow) and only a thin layer of structurally ill defined carbon is present on the exposed graphitic faces of the outer wall (Fig. 1c and d). Finally the annealing at 3000 °C results in a straightening of the graphitic sheets and highly graphitized walls which show connections between stacked cones, forming steps on the inner and outer surface which are decorated with some defective fullerene-like carbon (Fig. 1e and f), which is not observed after nitric acid treatment and ALD coating (see below). SEM images of the uncoated tubes are presented in Fig. SI10 in the ESI†.

The ALD of various metal oxides onto the CNT700 was recently reported. Briefly, it was shown that TiO_2, V_2O_4 and HfO_2 form a conformal and homogeneous amorphous film at deposition temperatures in the range between 50 and 250 °C.[9,10] On the other hand, it was found that the ALD of SnO_2 forms a granular film composed of sub-5 nm nanoparticles.[11] In this

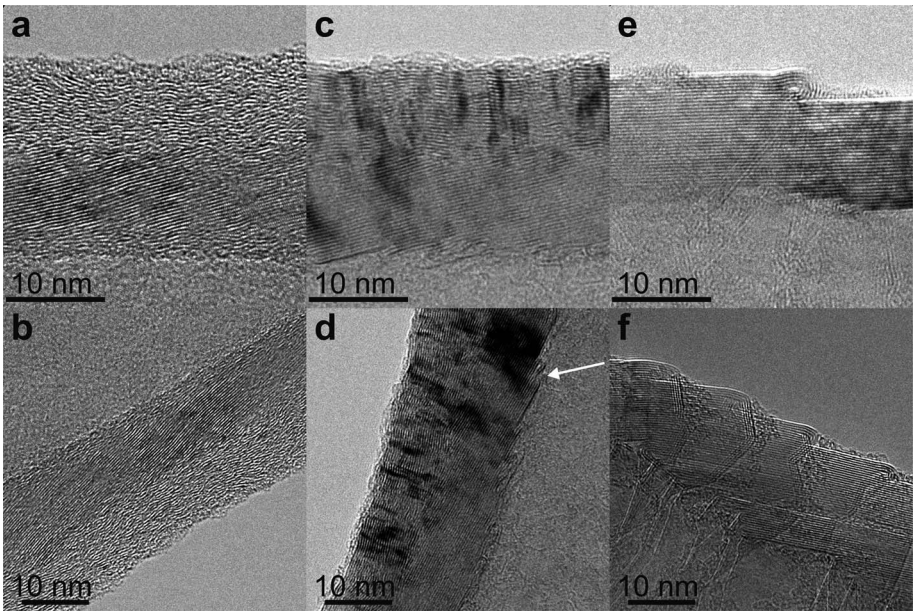

Fig. 1 HRTEM images of the different CNTs prior to TiO_2 ALD. CNT700 (a and b), CNT1500 (c and d) and CNT3000, the latter before nitric acid treatment (e and f).

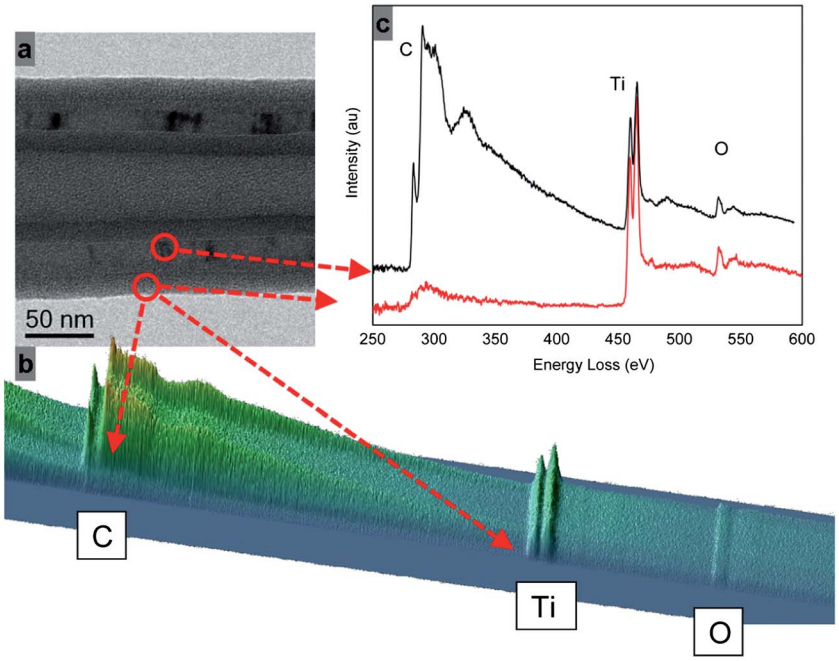

Fig. 2 (a) Shows the part of a TiO_2 coated CNT from where the EELS signal was recorded (film thickness ~ 16 nm). The recorded intensity is shown in (b) as a three-dimensional plot in the energy dispersive plane. It nicely reveals the development of the C-K, Ti-L and O-K edges across the tube. The EELS spectra abstracted from the coating (red) and from a region where signal is due to the film on the top and bottom surface plus the CNT walls (black) are shown in (c).

particular case, HRTEM studies revealed that the particulate film formation can be attributed to the property of SnO_2 to directly form crystalline nanoparticles during the deposition, even at temperatures as low as 150 °C. Indeed, the same particulate growth pattern was obtained for SnO_2 on silicon wafers passivated with native silicon oxide. However, independent of the metal oxide that was deposited on the tubes, it was generally observed that no growth occurs on exposed graphitic planes. It can therefore be concluded that the initiation of film growth requires defects and anchoring sites at the surface of the tube.

For the present study, TiO_2 ALD was chosen for the coating as it is known to lead to a very homogeneous growth of an amorphous film on the CNT700 and is therefore expected to be most suitable to detect small variations in the distribution of anchoring sites at high spatial resolution.

In order to analyze the chemical composition and purity of the deposited metal oxide, electron energy loss spectrometry (EELS) was used.[9] Intensity of the EELS spectrum recorded across the diameter of a coated tube and spectra abstracted at different positions are shown in Fig. 2. The figure reveals the development

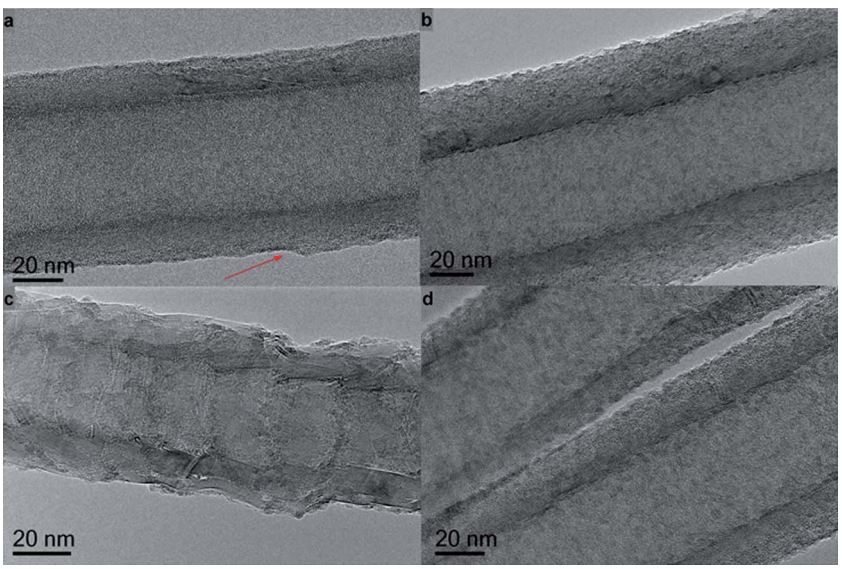

Fig. 3 Overview TEM images of CNTs coated with TiO_2 by ALD. (a) CNT700 (100 cycles), (b) CNT1500 (50 cycles), (c) CNT3000 (50 cycles), and (d) CNT700D (100 cycles).

of the Ti-L, O-K and C-K signal across the tube. Due to the high ionization cross-section for the carbon 1s electrons, EELS is very sensitive to carbon. This is evident from the spectrum corresponding to the central region of the tube, where the integrated area of the carbon signal dominates the spectrum. In the surface region, on the other hand, the spectrum shows a small carbon signal. Elemental quantification of the spectrum abstracted from the surface region reveals a carbon content of less than 5%. This is a rough estimate for the upper limit of carbon in the film since some carbon signal might also be due to the close proximity of the tube walls plus contamination due to exposure to ambient air. The shape and intensities of the Ti and O features in the EELS spectra fit to TiO_2. It must be stressed here that the shape and intensity of ionization edges in EELS are very sensitive to the local chemical surrounding of the ionized species. The correspondence of the shape to what is expected for TiO_2 therefore speaks for a high purity of the as-deposited film.

In each ALD deposition, the four differently functionalized tubes were coated simultaneously in the same chamber. As expected, a homogeneous thin film growth was observed on the surface of CNT700. This is shown in Fig. 3a for a film obtained after 100 ALD cycles. Slight variations of the contrast in the central region are due to the projection of thickness variations (dents and hills) and structural inhomogeneities in the amorphous carbon layer of the tube wall. The latter can be nicely seen on the outer surfaces of the wall. Contrast variations seen in the central region might also be due to inhomogeneities of the film itself. However, when looking at the surface regions where the electron beam passes perpendicular to the surface normal of the graphitic walls, the titania film is visible as a thin layer of darker contrast on the inner and outer surface of the tube. It follows smoothly all the hills and valleys of the tube surface in a conformal way and with relatively constant thickness (see arrow in Fig. 3a). SEM images for CNT700 coated with 65 TiO_2 ALD cycles support these findings (Fig. SI1†). The homogeneous contrast indicates a very smooth coating of the surface, which is only interrupted by occasional defects in the film (*cf.* also the SEM image of the uncoated tube in Fig. SI10a†). As compared to the morphology of the film on the CNT700, the TEM image of the CNT1500 reveals a more granular aspect (Fig. 3b). Indeed, a pronounced particulate structure can be seen on the inside and outside walls of the carbon material. The surface of the CNT3000 is characterized by steps running around the tube surface (*cf.* Fig. 1e and f). TEM investigation after ALD deposition reveals that the highly graphitic walls remain mostly uncoated, whilst TiO_2 deposition and growth can be observed at the cone edges (Fig. 3c). Finally, the coating of the CNT700 after partial defunctionalization (CNT700D) appears more granular than in the case of the CNT700 (Fig. 3d). As expected, this is a result of a reduction in the oxygen containing surface groups and hence, a reduced availability of anchoring sites.

At higher magnification, HRTEM imaging confirms the different and more granular aspect of the films grown on the CNT1500, CNT3000 and CNT700D tubes (Fig. 4–6 and ESI†) when compared to the smooth coating observed in the case of the CNT700. The particulate structure can nicely be seen on the inside and outside part of the carbon material for the CNT1500 (Fig. 4 and SI2†). Especially, at the outer CNT surface, where the

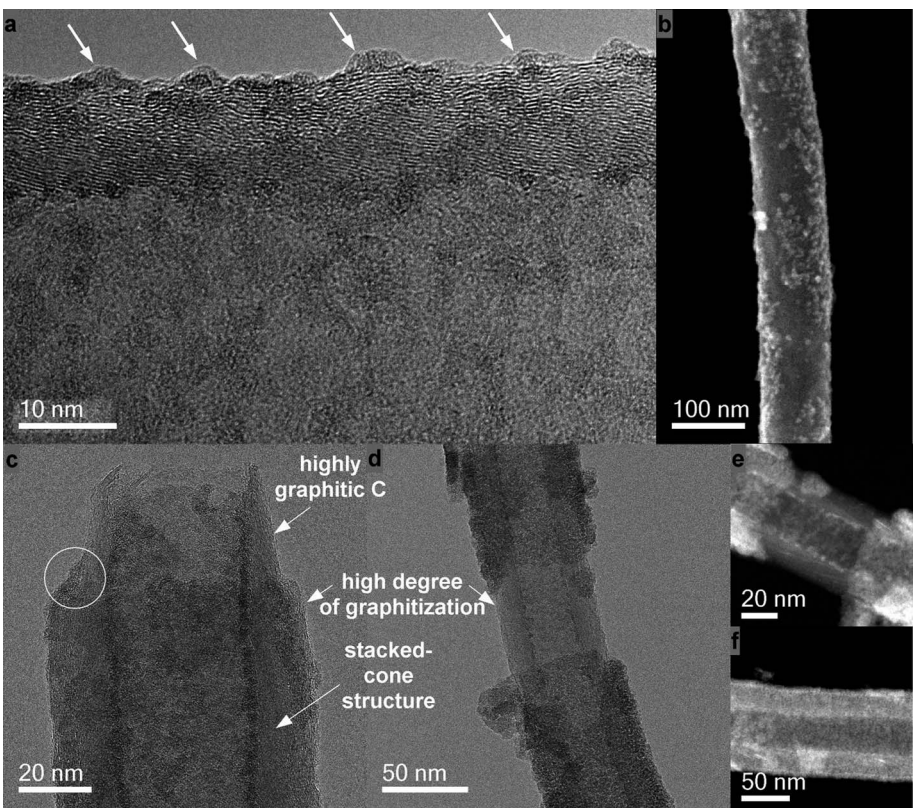

Fig. 4 HRTEM (a) and SEM (b) images recorded from the CNT1500 coated during 50 cycles. (c), (d) and (e), (f) show uncoated regions on tubes in HRTEM and HAADF-STEM images recorded from tubes coated during 100 cycles.

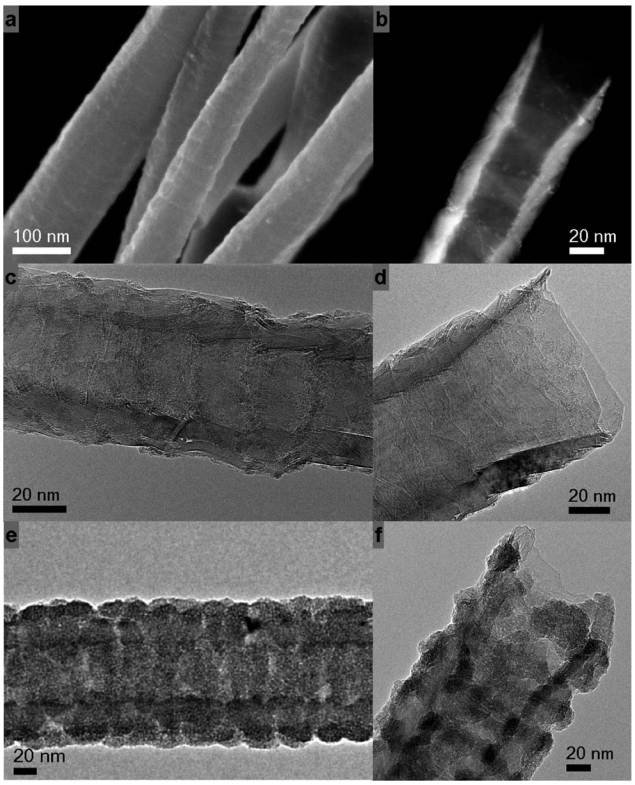

Fig. 5 (a) SEM, (b) HAADF-STEM, (c and d) HRTEM and (e and f) TEM images of the CNT3000 coated with (b) 25, (a, c and d) 50 and (e and f) 500 TiO_2 ALD cycles.

film can be observed without a disturbing background, the formation of titania clusters is clearly visible for the CNT1500 (arrows in Fig. 4a), for example. They measure a few nm in size and are grown onto the curved carbon crystallites, *i.e.* in defective areas. The same growth mode is also evident in the SEM image shown in Fig. 4b and SI2a†. It reveals titania particles as bright dots that are randomly distributed on the surface of the CNT. The SEM image also shows relatively large regions that remain completely uncoated. We have already shown that the precursor vapors used in the present ALD process are able to diffuse into small pores and lead to a complete coating even on the inside walls throughout long tubes. If we exclude mechanical peeling off of the film after deposition due to weak connections between the film and tube, we can conclude that regions that remain uncoated are either due to a covering of the respective region during the ALD process (touching tubes or connections with the support) or due to a lack of growth initiation events. This is consistent with previous observations that have shown that no growth occurs on defect free graphitic planes (*cf.* also Fig. 4c–f and HRTEM images for 100 and 500 TiO_2 ALD cycles in the ESI Fig. SI2b and c†).[11] It can therefore be concluded that the differences observed between the CNT700 and CNT1500 tubes in terms of the aspect of the coating are directly related to the different density and distribution of suitable initiation sites. At 1500 °C, the small graphitic domains or graphene sheets (BSUs) grow to form larger crystallites of sp^2-hybridized carbon.[36] Paredes *et al.* investigated the pristine cup-stacked CNTs used in the present work and they observed by scanning tunneling microscopy (STM) the formation of flat terraces after annealing at 1500 °C.[37] These domains are defect-free, hence they do not provide any anchoring point during the ALD of TiO_2. The latter is no longer able to grow as a film but instead it forms nanoparticles centered on defective areas, rich in O-containing surface functional groups.

In order to study the development of the growth mode, the number of deposition cycles was increased to 100 (Fig. 4c–f and SI2b†) and 500 (Fig. SI2c†). The initiation of the growth appears to follow an island growth that tends to transform to a 2-D growth with increasing number of cycles, leading to a homogenization of the thickness. This is already observed after 100 cycles (Fig. 4c–f and SI2b†). However, even in thick films, domains that remain uncoated can be found (Fig. SI2c†). Generally, uncoated regions are found at the endings of the tubes, where the catalytically grown graphitic surface is observed to protrude from the pyrolytic layer (sword-in-sheath failure), and, similarly, on the inner surface, in the region where the last stacked cone of the structure exposes graphitic planes. In analogy, uncoated areas observed along the tube surface are due to the absence of an anchoring site, preventing the initiation of film growth.

As demonstrated by HRTEM prior to ALD, the CNT3000 tubes show a particular structure made of steps, walls and flat terraces that are highly graphitic (*cf.* Fig. 1e and f), in agreement with Paredes *et al.* STM investigations.[37] Fig. 5a shows a SEM image of several CNTs coated during 100 ALD cycles. As expected, the exposed graphitic parts remain mostly undecorated, and deposition only takes place at the edges of connected cones. The reason for this is the high curvature at the edge, which

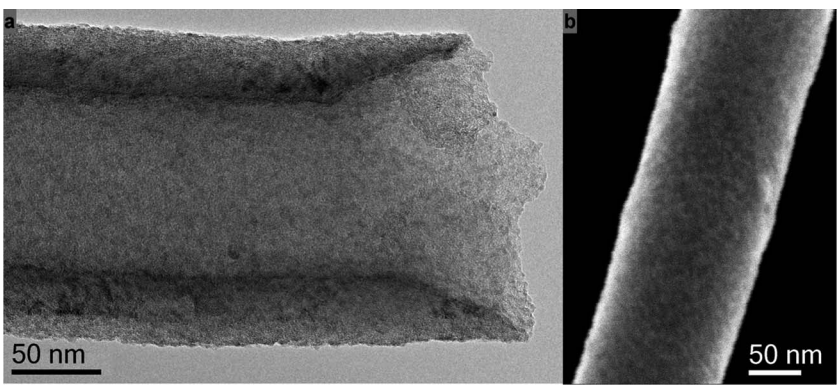

Fig. 6 HRTEM (a) and SEM (b) images of CNT700D coated with 50 TiO_2 ALD cycles.

involves the presence of structural defects (5-membered rings) and strained C–C double bonds. In these regions, the sp^2-hybridized carbon atoms easily react to become sp^3-hybridized and thus release the strain. HNO_3 is typically used to open SWCNTs and MWCNTs because it preferentially reacts with the curved tips of the tubes. Similarly, while the oxidizing power of HNO_3 is not strong enough (in our reaction conditions) to break C–C double bonds and functionalize the graphitic terraces, it reacts and creates O-containing functional groups on the curved graphene sheets between two cones. As a result of the preferential deposition at the edges, the ALD leads to rings of TiO_2 film wrapped around the CNTs. These structures are clearly visible on the high angle annular dark field (HAADF) scanning transmission electron microscopy (STEM) image (Fig. 5b and SI3†. Reference image before coating, see ESI†) and can also be seen in the HRTEM images (Fig. 5c–f and SI4–SI7†). The series of HRTEM images acquired from CNT3000 coated with a different number of TiO_2 ALD cycles, *i.e.* 50 (Fig. SI4 and SI5†), 100 (Fig. SI6†) and 500 (Fig. SI7†), clearly shows the defective regions where the TiO_2 growth initiates. From these observations it can be concluded that the acidic treatment on the high temperature (3000 °C) treated CNTs leads only to an oxidation at the edges, where the carbon sheets are highly curved or are abruptly terminated. The titania deposition demonstrates nicely this functionalization. At low magnification, TEM permits us to ascertain that these defects are homogeneously distributed all along the tubes. This is shown in Fig. SI8†, where two tubes present TiO_2 clusters that are related to the surface structure of the tubes (see edges in the SEM image of Fig. 5a).

Similarly to the case of the CNT1500, coating of the defunctionalized tubes (CNT700D) leads to a granular aspect of the film (Fig. 6 and SI9†). The particulate structure is nicely observed on the inside and outside part of the carbon material. Compared to the CNT1500, the average particle size is slightly smaller and the coating more homogeneous. Especially, the SEM and STEM images (Fig. 6b and SI9a†) show that the particle density is higher and more regular, *i.e.*, without large regions that remain completely uncoated. This observation is consistent with the X-ray photoelectron spectroscopy (XPS) analysis of both supports prior to ALD. Here, the O/C ratios determined from XPS spectra for the CNT1500 and CNT700D are very similar, *i.e.* 0.012 and 0.011, respectively (*cf.* Table 1 and ref. 27). It can be concluded that for the CNT1500 support, defective areas with a high concentration of O-containing groups are dispersed within a patchwork of (unfunctionalized) graphitic regions. In contrast, for the CNT700D support, the oxygen concentration is lower but the groups are more homogeneously dispersed throughout the surface. This is also confirmed by a series of HRTEM images acquired after coating with 0 up to 1000 cycles of TiO_2 ALD (Fig. 6a and SI9b–e†). After many ALD cycles, the film becomes conformal due to the transition from an island to a 2D growth mode. This is in contrast to what is observed for the CNT1500 support, where the coating does not reach the same degree of conformality and remains rough. Electron microscopic investigation furthermore reveals that the large uncoated regions, frequently observed in the case of the CNT1500 support, are absent in the case of the CNT700D tubes.

The XPS analysis of the pristine cup-stacked carbon nanotubes, as well as of commercial multiwalled carbon nanotubes (NC-3100 from Nanocyl and Baytubes from Bayer), revealed that even untreated carbon nanomaterials exhibit O-containing functional groups on their surface.[38] These groups were formed when the materials were exposed to air after synthesis, as their defects reacted with O_2 and H_2O.[39] The calculated O/C ratio for the pristine nanocarbons ranged between 0.005 and 0.034, similar to the O/C ratios found for CNT700D, CNT1500 and CNT3000. We therefore expect to be also able to map the defects in any nanocarbon, without any additional chemical treatment, by ALD. Preliminary experiments on the pristine cup-stacked CNTs and on pristine MWCNTs were conclusive.

The requirement of the presence of anchoring sites for the initiation of film growth in ALD makes this method, in combination with HRTEM imaging, suitable to study the spatial distribution of functional sites on high surface area supports. In fact, ALD appears as the technique of choice to map anchoring sites on nanostructured supports and to study the distribution of functional groups as a function of structure and functionalization treatment. In comparison, Raman spectroscopy does not offer a spatial resolution high enough to map the defects at the nm scale. Alternative techniques such as STM that provide atomic resolution are limited in the study of complex nanostructured materials and allow only scanning a small region of the sample.

Conclusions

In this manuscript it was shown that the growth modes of TiO_2 ALD onto CNTs strongly depend on the different chemical and thermal treatments of the substrate. 2D and island growth modes could be tuned by the surface functionalization of the CNTs as well as the transition from island to 2D mode, which depend on the number of ALD cycles. In the case of high temperature treated stacked-cup nanotubes, a peculiar ring nanostructured coating could be obtained due to the pattern of the surface functional groups induced by the chemical and thermal treatments. All in all, it was shown that atomic layer deposition provides a means to specifically label anchoring sites and that it can be used to characterize the spatial distribution of surface functionality of differently treated carbon nanotubes. Finally, the approach introduced in the present work can certainly be applied to various carbon nanostructures and other nanostructured surfaces in general.

We foresee that the labeling of defects in nanocarbons by ALD will play a role in better understanding the relation between structure and defects as well as their relation to the physical and electronic properties like, for example, in the study of the grain boundaries in graphene.[40] In addition, we believe that ALD will help to understand why MWCNTs which seem to be structurally similar exhibit different chemical, physical and electronic properties.[41]

Acknowledgements

This work was partially supported by the WCU (World Class University) program through the National Research Foundation (NRF) of Korea funded by the Ministry of Education, Science and Technology (R31-10013) and FCT projects (PTDC/CTM/098361/2008), (PTDC/CTM/100468/2008), (REDE/1509/RME/2005) and (SFRH/BD/71453/2010).

References

1 M. Leskelä and M. Ritala, *Angew. Chem., Int. Ed.*, 2003, **42**, 5548–5554.
2 S. M. George, *Chem. Rev.*, 2010, **110**, 111–131.
3 R. L. Puurunen, *J. Appl. Phys.*, 2005, **97**, 121301–121352.
4 M. Knez, K. Nielsch and L. Niinistö, *Adv. Mater.*, 2007, **19**, 3403–3419.
5 *Atomic Layer Deposition of Nanostructured Materials*, ed. N. Pinna and M. Knez, Wiley-VCH, 2011.
6 C. Marichy, M. Bechelany and N. Pinna, *Adv. Mater.*, 2012, **24**, 1017–1032.
7 C. Marichy, A. Pucci, M.-G. Willinger and N. Pinna, in *Atomic Layer Deposition of Nanostructured Materials*, ed. N. Pinna and M. Knez, Wiley-VCH, 2011.
8 A. S. Cavanagh, C. A. Wilson, A. W. Weimer and S. M. George, *Nanotechnology*, 2009, **20**, 255602.
9 M. G. Willinger, G. Neri, A. Bonavita, G. Micali, E. Rauwel, T. Herntrich and N. Pinna, *Phys. Chem. Chem. Phys.*, 2009, **11**, 3615–3622.
10 M. G. Willinger, G. Neri, E. Rauwel, A. Bonavita, G. Micali and N. Pinna, *Nano Lett.*, 2008, **8**, 4201–4204.
11 C. Marichy, N. Donato, M.-G. Willinger, M. Latino, D. Karpinsky, S.-H. Yu, G. Neri and N. Pinna, *Adv. Funct. Mater.*, 2011, **21**, 658.
12 D. B. Farmer and R. G. Gordon, *Electrochem. Solid-State Lett.*, 2005, **8**, G89–G91.
13 D. B. Farmer and R. G. Gordon, *Nano Lett.*, 2006, **6**, 699–703.
14 C. F. Herrmann, F. H. Fabreguette, D. S. Finch, R. Geiss and S. M. George, *Appl. Phys. Lett.*, 2005, **87**, 123110.
15 J. S. Lee, B. Min, K. Cho, S. Kim, J. Park, Y. T. Lee, N. S. Kim, M. S. Lee, S. O. Park and J. T. Moon, *J. Cryst. Growth*, 2003, **254**, 443–448.
16 G.-D. Zhan, X. Du, D. M. King, L. F. Hakim, X. Liang, J. A. McCormick and A. W. Weimer, *J. Am. Ceram. Soc.*, 2008, **91**, 831–835.
17 Y.-S. Min, E. J. Bae, J. B. Park, U. J. Kim, W. Park, J. Song, C. S. Hwang and N. Park, *Appl. Phys. Lett.*, 2007, **90**, 263104.
18 X. Wang, S. M. Tabakman and H. Dai, *J. Am. Chem. Soc.*, 2008, **130**, 8152–8153.
19 S. Banerjee, T. Hemraj-Benny and S. S. Wong, *Adv. Mater.*, 2005, **17**, 17–29.
20 A. Hirsch, *Angew. Chem., Int. Ed.*, 2002, **41**, 1853–1859.
21 Y. Fan, B. R. Goldsmith and P. G. Collins, *Nat. Mater.*, 2005, **4**, 906–911.
22 X. Li, J. Niu, J. Zhang, H. Li and Z. Liu, *J. Phys. Chem. B*, 2003, **107**, 2453–2458.
23 X. Wang, L. Cao, C. E. Bunker, M. J. Meziani, F. Lu, E. A. Guliants and Y.-P. Sun, *J. Phys. Chem. C*, 2010, **114**, 20941–20946.
24 Y. Fan, M. Burghard and K. Kern, *Adv. Mater.*, 2002, **14**, 130–133.
25 M. S. Dresselhaus, G. Dresselhaus, R. Saito and A. Jorio, *Phys. Rep.*, 2005, **409**, 47–99.
26 G. G. Tibbetts, M. L. Lake, K. L. Strong and B. P. Rice, *Compos. Sci. Technol.*, 2007, **67**, 1709–1718.
27 J.-P. Tessonnier, D. Rosenthal, F. Girgsdies, J. Amadou, D. Begin, C. Pham-Huu, D. S. Su and R. Schlögl, *Chem. Commun.*, 2009, 7158–7160.
28 E. Rauwel, G. Clavel, M. G. Willinger, P. Rauwel and N. Pinna, *Angew. Chem., Int. Ed.*, 2008, **47**, 3592–3595.
29 J.-P. Tessonnier, O. Ersen, G. Weinberg, C. Pham-Huu, D. S. Su and R. Schlögl, *ACS Nano*, 2009, **3**, 2081–2089.
30 D. Shuai, C. Wang, A. Genc and C. J. Werth, *J. Phys. Chem. Lett.*, 2011, **2**, 1082–1087.
31 W. Zheng, J. Zhang, B. Zhu, R. Blume, Y. Zhang, K. Schlichte, R. Schlögl, F. Schüth and D. S. Su, *ChemSusChem*, 2010, **3**, 226–230.
32 B. Li, C. Wang, G. Yi, H. Lin and Y. Yuan, *Catal. Today*, 2011, **164**, 74–79.
33 C. G. Salzmann, S. A. Llewellyn, G. Tobias, M. A. H. Ward, Y. Huh and M. L. H. Green, *Adv. Mater.*, 2007, **19**, 883–887.
34 A. Rinaldi, J. Zhang, B. Frank, D. S. Su, S. B. Abd Hamid and R. Schlögl, *ChemSusChem*, 2010, **3**, 254–260.
35 M. Endo, Y. A. Kim, T. Hayashi, T. Yanagisawa, H. Muramatsu, M. Ezaka, H. Terrones, M. Terrones and M. S. Dresselhaus, *Carbon*, 2003, **41**, 1941–1947.
36 R. Schlögl, in *Handbook of Heterogeneous Catalysis*, ed. G. Ertl, H. Knözinger, F. Schüth and J. Weitkamp, Wiley VCH, Weinheim, 2007.
37 J. I. Paredes, M. Burghard, A. Martínez-Alonso and J. M. D. Tascón, *Appl. Phys. A: Mater. Sci. Process.*, 2005, **80**, 675–682.
38 J.-P. Tessonnier, D. Rosenthal, T. W. Hansen, C. Hess, M. E. Schuster, R. Blume, F. Girgsdies, N. Pfänder, O. Timpe, D. S. Su and R. Schlögl, *Carbon*, 2009, **47**, 1779–1798.
39 R. Menzel, M. Q. Tran, A. Menner, C. W. M. Kay, A. Bismarck and M. S. P. Shaffer, *Chem. Sci.*, 2010, **1**, 603–608.
40 P. Y. Huang, C. S. Ruiz-Vargas, A. M. van der Zande, W. S. Whitney, M. P. Levendorf, J. W. Kevek, S. Garg, J. S. Alden, C. J. Hustedt, Y. Zhu, J. Park, P. L. McEuen and D. A. Muller, *Nature*, 2011, **469**, 389–392.
41 E. P. J. Parrott, J. A. Zeitler, J. McGregor, S.-P. Oei, H. E. Unalan, W. I. Milne, J.-P. Tessonnier, D. S. Su, R. Schlögl and L. F. Gladden, *Adv. Mater.*, 2009, **21**, 3953–3957.